A statistical analysis of exhaled respiratory droplet trajectory distribution in view of assessing the risk of infectious disease transmission

M Cavazzuti[1], L Campanelli[1] and P Tartarini[2]

[1] Dipartimento di Scienze e Metodi dell'Ingegneria, Università degli Studi di Modena e Reggio Emilia, via Giovanni Amendola 2, Reggio Emilia, 42122, Italia
[2] Dipartimento di Ingegneria "Enzo Ferrari", Università degli Studi di Modena e Reggio Emilia, via Pietro Vivarelli 10, Modena, 41125, Italia

E-mail: marco.cavazzuti@unimore.it

Abstract. In the present work an analytical model of exhaled droplet trajectory and evaporation is employed to perform a preliminary statistical analysis of the droplet spatial distribution. The analysis is carried out for a set of over twenty thousand droplets distributed in the range of diameters from 0.1 µm to 1 mm. The type of respiratory events modelled are mouth breathing and speaking. The analytical model employed has been recently developed by the authors. It implements the fundamental laws of fluid dynamics and convection-diffusion, and features a 2D empirical numerical model of buoyant intermittent jet modelling the exhaled breath cloud. A discrete random walk turbulent dispersion model is also included allowing statistical analysis of the droplet trajectory to be performed. With proper boundary conditions any type of respiratory event can be simulated making the model particularly versatile. From the analysis, spatial virus concentration maps are derived for the largest droplets falling to the ground, and for the smaller droplets remaining airborne in the area in front of an infected emitter and successively uniformly dispersed in the ambient. This allows to estimate the risk of infection by fomite, direct inhalation and indirect inhalation routes, and provide a better understanding of infectious disease transmission risks.

1. Introduction

Infectious diseases are primarily transmitted from host to host through tiny pathogen-laden droplets exhaled during respiratory events such as breathing, speaking, coughing, or sneezing. These droplets can have very different size ranging from the sub-micron scale up to approximately one millimetre. Depending on their dimension and on the thermo-hygrometric conditions of the surrounding environment, droplets may either fall to the ground while evaporating or remain suspended in the air after evaporation. In both cases any virus that may be carried along can survive from several hours up to several days so that the infectious disease can be transmitted to the airways of a susceptible host either indirectly through contact with an infected surface, or through direct inhalation of the airborne droplet nucleus made of salts, protein, and eventually viruses.

From an analytical point of view, the trajectory and the evaporation of the droplets are governed by the fundamental laws of fluid dynamics and by convection-diffusion equation. Further, the modelling of the droplet transport cannot ignore the role of the breath cloud,

a buoyant intermittent jet from which smaller droplets may not be able to escape and that can quickly carry them far from where they have been originated.

In the literature the issue has been addressed in several ways, ranging from discrete phase model CFD analyses, to analytical models of droplet transport and evaporation, to statistical infection models based on virion concentration and exposure time [1, 2]. In [3] the CFD model of a sneeze is presented, while a cough is investigated in [4]. In [5] the droplet transport and dispersion due to ventilation in a room is modelled by means of CFD for a given vents layout. An analytical model of the droplet transport and evaporation within a continuous jet breath cloud is given in [6], while in [7] a similar model is presented where the breath cloud buoyancy is included and turbulent dispersion modelled with a discrete random walk stochastic approach. The work in [8] highlights how the breath cloud should rather be modelled as a sequence of jet and puff phases as these have different spatial evolution in time. In [9] a map of the distance travelled by droplets of different size and initial velocity is given, while in [10] another map is introduced estimating the chance, for droplets of different size, of being either inhaled or deposited on facial mucous membranes in function of a generic relative distance from the exhalation source for the case of a cough. The two works are based on simplified analytical model of the droplet transport and evaporation within the breathing cloud modelled as a jet.

In the recent past, the authors have developed an analytical model of the exhaled droplet transport and evaporation, implemented in Python language. Besides solving the basic transport and evaporation equations, the model solves the energy equation, and addresses the role of non-volatile components on the droplet evaporation. Further, it implements a one-dimensional numerical model of the buoyant breath cloud based on momentum conservation equation where the cloud is modelled as composed by a periodic sequence of jet and puff phases.

The analytical model has been lately enriched with additional features such as the ability of modelling a non-uniform exhaled breath velocity profile in time and in space, the randomisation of the initial droplet position within the inlet surface representing the mouth or the nose, and the randomisation of the droplet injection time within the exhalation time span of the respiratory event being modelled. Last, a discrete random walk model has been added to mimic the effect of turbulent dispersion on the local droplet trajectory. First of all, these features allow a more accurate modelling of the breath cloud. Further, the addition of the random elements mentioned above enables statistical analyses of the droplet trajectory to be performed.

To be noted that the analytical model only simulates isolated droplets and does not address droplet to droplet interactions as these has been shown to be irrelevant for the case of respiratory exhalations due to the low droplet concentration found [11].

In the current work, this analytical model has been used to perform a preliminary statistical analysis on the trajectory distribution of droplets of various sizes ranging from 0.1 µm to 1 mm for the cases of periodic mouth breathing and speaking. By assuming the viral load of the saliva, trajectory information can be used to derive spatial risk maps that estimates the virus concentration in the ambient and the risk of inhaling a certain dose of virus while remaining for a lapse of time in close contact or in the same ambient with a breathing or speaking infected individual. The map could provide a more solid background to the social distancing rule that we all became acquainted with during the recent SARS-CoV-2 pandemic, and could help in improving the understanding of infectious diseases transmission and prevent their diffusion.

2. Analytical model

2.1. Transport

The droplet, during its flight, is subject to weight ($\mathcal{W}$) and drag ($\mathcal{D}$) forces. Including buoyancy in the weight term, these can be written as

$$\begin{aligned} \mathcal{W} &= \tfrac{1}{6}\left(\rho_\mathrm{p}-\rho_\mathrm{s}\right)\pi D_\mathrm{p}\,\mathbf{g} \\ \mathcal{D} &= -\tfrac{1}{8}C_\mathrm{d}\rho_\mathrm{s}\pi D_\mathrm{p}^2\left\|\mathbf{u}_\mathrm{r}\right\|\,\mathbf{u}_\mathrm{r} \end{aligned} \tag{1}$$

where ρ is the density, D the diameter, $\mathbf{g}$ the gravitational acceleration vector, C_d the drag coefficient, and $\mathbf{u}_\mathrm{r}$=$\mathbf{u}_\mathrm{p}$−$\mathbf{u}_\infty$ the relative velocity vector between the droplet and the local undisturbed air flow. Subscript "p" denotes the droplet or particle and "s" the air by the droplet surface. From Newton's second law, for a generic horizontal direction x and vertical direction z, the droplet relative acceleration is

$$\begin{cases} \dot{u}_\mathrm{r,x} = \frac{\mathcal{D}_\mathrm{x}}{m_\mathrm{p}} = -\frac{u_\mathrm{r,x}}{\tau_\mathrm{d}} \\ \dot{u}_\mathrm{r,z} = \frac{\mathcal{W}_\mathrm{z}+\mathcal{D}_\mathrm{z}}{m_\mathrm{p}} = \frac{u_\mathrm{r,t}}{\tau_\mathrm{d,t}} - \frac{u_\mathrm{r,z}}{\tau_\mathrm{d}} \end{cases} \tag{2}$$

where m is the mass and τ_d the drag characteristic time

$$\tau_\mathrm{d} = \frac{m_\mathrm{p}u_\mathrm{r,z}}{\mathcal{D}_\mathrm{z}} = \frac{4\rho_\mathrm{p}D_\mathrm{p}}{3C_\mathrm{d}\rho_\mathrm{s}\left\|\mathbf{u}_\mathrm{r}\right\|} \tag{3}$$

The subscript "t" denotes the terminal condition, *i.e.* the condition the droplet will attain in the limit, when $\dot{\mathbf{u}}_\mathrm{r}$=$\mathbf{0}$

$$u_\mathrm{r,t} = -\sqrt{\frac{4g_\mathrm{z}D_\mathrm{p}}{3C_\mathrm{d,t}}\left(\frac{\rho_\mathrm{p}}{\rho_\mathrm{s}}-1\right)} = -\left(1-\frac{\rho_\mathrm{s}}{\rho_\mathrm{p}}\right)g_\mathrm{z}\tau_\mathrm{d,t} \tag{4}$$

For the special case of Stokes' flow, *i.e.* when the Reynolds number Re≪1, C_d=24/Re and τ_d=$\tau_\mathrm{d,t}$=$(\rho_\mathrm{p}D_\mathrm{p}^2)/(18\mu_\mathrm{s})$, where μ is the dynamic viscosity. Otherwise a correlation is needed to estimate the drag coefficient as a function of the Reynolds number. By integrating equation (2) twice with initial conditions $\mathbf{u}_\mathrm{r,0}$ and $\mathbf{s}_\mathrm{p,0}$ the droplet velocity and its trajectory are found as

$$\begin{cases} u_\mathrm{p,x}\left(t\right) = u_\mathrm{\infty,x} + u_\mathrm{r,x,0}\mathrm{e}^{-t/\tau_\mathrm{d}} \\ u_\mathrm{p,z}\left(t\right) = u_\mathrm{\infty,z} + u_\mathrm{r,z,0}\mathrm{e}^{-t/\tau_\mathrm{d}} + u_\mathrm{r,t}\frac{\tau_\mathrm{d}}{\tau_\mathrm{d,t}}\left(1-\mathrm{e}^{-t/\tau_\mathrm{d}}\right) \end{cases} \tag{5}$$

and

$$\begin{cases} s_\mathrm{p,x}\left(t\right) = s_\mathrm{p,x,0} + u_\mathrm{\infty,x}t + u_\mathrm{r,x,0}\tau_\mathrm{d}\left(1-\mathrm{e}^{-t/\tau_\mathrm{d}}\right) \\ s_\mathrm{p,z}\left(t\right) = s_\mathrm{p,z,0} + \left(u_\mathrm{\infty,z} + u_\mathrm{r,t}\frac{\tau_\mathrm{d}}{\tau_\mathrm{d,t}}\right)t + \left(u_\mathrm{r,z,0} - u_\mathrm{r,t}\frac{\tau_\mathrm{d}}{\tau_\mathrm{d,t}}\right)\tau_\mathrm{d}\left(1-\mathrm{e}^{-t/\tau_\mathrm{d}}\right) \end{cases} \tag{6}$$

2.2. Evaporation

Mass transfer from the droplet to the ambient due to evaporation follows convection-diffusion equation. Without the source term and neglecting the diffusion of air in water, with a few algebraic passages this can be reformulated in terms of droplet diameter reduction rate as

$$\dot{D}_\mathrm{p} = -\frac{K}{2D_\mathrm{p}} = -\frac{2D_\mathrm{v,s}\mathrm{Sh}}{\rho_\mathrm{p}D_\mathrm{p}R_\mathrm{v}T_\mathrm{p}}\frac{p}{p_\mathrm{a,s}}\left(p_\mathrm{v,s}-p_\mathrm{v,\infty}\right) \tag{7}$$

where K is the evaporation rate, D_v the mass diffusivity of water in air, Sh the Sherwood number, R the specific gas constant, T temperature, and p pressure. Subscript "v" denotes the water vapour and "a" the dry air. While the droplet is evaporating, the air surrounding the droplet surface can be assumed as saturated and its temperature equal to that of the droplet in order to compute the water vapour partial pressure by the droplet surface $p_{\mathrm{v,s}}$. By integrating equation (7) with initial condition $D_{\mathrm{p},0}$

$$D_\mathrm{p}\left(t\right) = \sqrt{D_{\mathrm{p},0}^2 - Kt} \tag{8}$$

is found.

2.3. Energy balance

In terms of energy balance, the droplet sensible thermal power is balanced by convective heating and evaporative cooling. Putting these elements together, the balance can be reformulated in terms of droplet temperature rate of change as

$$\dot{T}_\mathrm{p} = \frac{T_\mathrm{s,t} - T_\mathrm{p}}{\tau_\mathrm{e}} \tag{9}$$

where τ_e is the evaporation characteristic time

$$\tau_\mathrm{e} = \frac{c_\mathrm{p}\rho_\mathrm{p}D_\mathrm{p}^2}{6\lambda_\mathrm{s}\mathrm{Nu}} \tag{10}$$

and

$$T_\mathrm{s,t} = T_\infty - \frac{h_\mathrm{lt}\rho_\mathrm{p}K}{4\lambda_\mathrm{s}\mathrm{Nu}} \tag{11}$$

the droplet terminal temperature, *i.e.* the ambient wet bulb temperature. In the equations above c is the specific heat, λ the thermal conductivity, Nu the Nusselt number, h_lt the water latent heat of vaporisation. By integrating equation (9) with initial condition $T_{\mathrm{p},0}$ droplet temperature can be written as

$$T_\mathrm{p}\left(t\right) = T_{\mathrm{p},0}\mathrm{e}^{-t/\tau_\mathrm{e}} + T_\mathrm{s,t}\left(1 - \mathrm{e}^{-t/\tau_\mathrm{e}}\right) \tag{12}$$

Radiative heat transfer between the droplet and the surroundings can be included with little effort and without changes to the equations above, given that Nusselt number is computed including both convective and radiative contributions in the heat transfer coefficient. Nonetheless, thermal radiation is mostly negligible and in the present study is not addressed. In fact, if the droplet is assumed as a diffuse gray surface in a large cavity, a radiative heat transfer coefficient of $\approx$5.5 $\mathrm{W/m^2\,K}$ can be estimated at ambient temperature. On the contrary, from the well known Ranz-Marshall correlation, convective heat transfer coefficient is always $>0.052/D_\mathrm{p}$, and thus much larger than its radiative counterpart.

2.4. Non-volatile fraction

In case the droplet contains some non-volatile solid fraction, ρ_p and c_p terms appearing in previous equations must be computed as proper weighted averages between the two phases. From Raoult's law $p_{\mathrm{v,s}}$ term in equation (7) is reduced by a factor equal to the droplet liquid molar fraction y_l so that evaporation will terminate before the droplet is completely dried out, *i.e.* when $y_\mathrm{l}{=}p_{\mathrm{v},\infty}/p_{\mathrm{v,s}}$.

2.5. Breath cloud model

Respiratory droplets are exhaled within the breath cloud, a humid air environment that protects them from evaporation and favours their transport. From previous equations, it is apparent how local air velocity and thermohygrometric conditions play a fundamental role on the droplet fate. It is thus important to couple the analytical model outlined above with a breath cloud model.

Yet, a simple rigorous and universal way to build such a model does not exist due to the inherent complexity and the unsteady 3D nature of buoyant intermittent jets. The model proposed here takes hint from momentum conservation equation and several empirical models suggested in the literature on steady jets to account for the jet entrainment, buoyancy, and velocity profile.

It is assumed that the breath cloud cone grows radially from the mouth with an entrainment coefficient β, whose value is typically $\approx$0.1 [12] so that the cone semi-aperture at a generic radial distance r from the cone tip is βr. The cloud thermodynamic properties change with the radial distance from the mouth as the result of the mixing between the two streams given by exhaled and entrained air. Let us consider a steady jet: if momentum flux is conserved at each downstream radial section, the velocity u at a generic distance ξ from the mouth decreases as

$$\frac{u\left(\xi\right)}{u_0} = \frac{1}{\xi}\sqrt{\frac{\rho_0}{\rho\left(\xi\right)}} \tag{13}$$

where ξ=r/r_0 is the non-dimensional distance from the imaginary breath cloud cone tip, and r_0 the tip to mouth distance. Subscript "0" identifies the mouth section, having non-dimensional coordinate ξ=1. Similarly the cloud mass flow rate grows with the distance as

$$\frac{\dot{m}\left(\xi\right)}{\dot{m}_0} = \xi\sqrt{\frac{\rho\left(\xi\right)}{\rho_0}} \tag{14}$$

The jet velocity profile is bell-shaped, a normal Gaussian profile is commonly suggested in the literature [10, 13]

$$\frac{u\left(\xi,\zeta\right)}{u\left(\xi,0\right)} = \mathrm{e}^{-\zeta^2} \tag{15}$$

where ζ=$b/(\beta r)$ is the non-dimensional radial distance from the jet centreline over the section, and $u(1,0)$=u_0. This means the jet influence is perceived also beyond the cone aperture identified by β, even if marginally. A potential core length of $6.2d_\mathrm{m}$ is assumed where no entrainment occurs [10, 14], *i.e.* the velocity profile and the thermophysical properties of the jet do not vary, d_m being the mouth or nose equivalent cross-section diameter; ξ quantity is recomputed as necessary in the equations above so as to address this feature. To account for the unsteady and periodic nature of respiratory events in a simple way, it is assumed that the velocity in equation (13) is multiplied by a scaling factor $\gamma(t)$ computed so as to grant momentum conservation. With a few algebraic passages this translates into

$$\gamma\left(t\right) = \frac{\frac{P(t)}{\dot{P}_\mathrm{st}}}{\sqrt{2\int_0^t \frac{P(t)}{\dot{P}_\mathrm{st}}\mathrm{d}t}} \tag{16}$$

where $P(t)$ is the cumulative momentum injected from the beginning of the respiratory event

$$P\left(t\right) = \int_0^t \dot{P}\left(t\right)\mathrm{d}t \tag{17}$$

and $\dot{P}_\mathrm{st}$ the momentum flux injected by an equivalent steady and uniform jet characterised by u_0 velocity at the nozzle. Equation (16) applies to any exhaled velocity impulse in time.

Respiratory events are characterised by a quick rise in the exhaled velocity and a slower decay [3]. Here a piecewise-defined positive sinusoidal impulse is assumed having different angular velocities in the ascending and in the descending phases, and null velocity after the end of the exhalation.

Further, once the quantity $P(t)/\dot{P}$ is known, an exponential momentum decay rate $\mathrm{e}^{-t/\tau_\mathrm{j}}$ can be applied to it so as to account for the jet momentum dissipation, where τ_j is a characteristic dissipation time. The integral in equation (16) and the value of $\gamma(t)$ can then be recomputed accordingly.

The cloud buoyancy is modelled with an empirical correlation proposed in the literature [15]

$$\frac{z}{\sqrt{A_0}} = 0.0354\,\mathrm{Ri}_0 \left(\frac{x}{\sqrt{A_0}}\right)^3 \sqrt{\frac{T_0}{T_\infty}} \tag{18}$$

where z is the vertical offset of the jet centreline at a distance x from the mouth, A and Ri the cross-section area and the Richardson number at the mouth, respectively. The non-dimensional distance ξ is thus computed on the curved path defined by equation (18).

2.6. Turbulent dispersion

Turbulent dispersion is modelled through a discrete random walk model mimicking the droplet interaction with a sequence of turbulent eddies. Turbulence is assumed isotropic so that the droplet velocity perturbation along the three coordinate directions results

$$\mathbf{u}' = \boldsymbol{\epsilon}\sqrt{\frac{2k}{3}} \tag{19}$$

where k is the turbulent kinetic energy at the droplet location, and $\boldsymbol{\epsilon}$ a normally distributed random number vector. The velocity perturbation is to be added to the u_∞ term in equations (5) and (6), and is updated at interval of times equal to the minimum between the characteristic eddy lifetime t_l and the droplet eddy crossing time t_c

$$t_\mathrm{l} = 0.3\frac{k}{\varepsilon} \qquad , \qquad t_\mathrm{c} = -\tau_\mathrm{d} \ln\left(1 - \frac{l_\mathrm{e}}{\tau_\mathrm{d}\,\|\mathbf{u}_\mathrm{r}\|}\right) \tag{20}$$

where l_e=$0.164k^{1.5}/\varepsilon$ is the eddy length scale. From the equations above, it is clear how an estimate of the k and ε fields in the breath cloud jet is needed to evaluate both the entity of the velocity perturbation and its update time. Here the equations proposed in [13] are adopted

$$k = u\,(\xi,0)^2\, c_1 \left(\mathrm{e}^{-c_2(\zeta-c_3)^2} + \mathrm{e}^{-c_2(\zeta+c_3)^2}\right) \quad , \quad \varepsilon = \frac{u\,(\xi,0)^3}{\beta\xi r_0} c_4 \left(\mathrm{e}^{-c_5(\zeta-c_6)^2} + \mathrm{e}^{-c_5(\zeta+c_6)^2}\right) \tag{21}$$

where c_1=0.0667, c_2=1.079, c_3=0.6853, c_4=0.0178, c_5=1.963, and c_6=0.6126. Similar formulas, with slightly different coefficients are found in other works in the literature.

3. Simulations

The analytical model briefly outlined in §2 has been employed to perform a preliminary statistical analysis of droplet distribution. Mouth breathing and speaking cases are modelled, these are the more complicated scenarios to be addressed due to their periodic nature. Further, their slow exhalation velocity makes the role of buoyancy particularly relevant. The simulation conditions are as follows. The ambient air is assumed quiescent and at atmospheric pressure, its temperature and relative humidity being 20 °C and 50%. The mouth diameter is 2 cm and the exhaled jet is released horizontally. A tidal volume of 0.5 litres per breath is assumed with a

period of 4 s. The exhaled velocity has a peak at 0.6 s within the period, and terminates at 2.4 s. The breath temperature and relative humidity are 34 °C and 95%, while the jet entrainment coefficient is 0.1. Exhaled droplets are assumed to have a volume solid fraction of 1%, the solid fraction being characterised by density of 1200 kg/m^3, specific heat of 1100 J/kgK, and molar mass of 100 kg/kmol. Droplets with an initial temperature of 34 °C are randomly released during the exhalation time with a random initial position within the mouth cross-section area. The mouth is located at a height of 1.5 m from the ground. Droplets initial velocity is aligned with the breath cloud direction, and equals in modulus the 95% of the breath cloud velocity at their release time and position.

The model features include: droplet evaporation, cloud transport, cloud buoyancy, turbulent diffusion, cloud velocity profile Gaussian in space and piecewise sinusoidal in time, random droplet release, breath cloud jet potential core, 3D droplet trajectory modelling. Breath cloud momentum dissipation model has been momentarily switched off in favour of safety as this would result in a cloud able to penetrate further the ambient in front of the emitter.

A set of 972 logarithmically distributed droplet diameters, in the 0.1 µm-1 mm range, is simulated. Simulations are repeated 22 times for each diameter, for a total of over 21 thousand runs.

In order to create potential risk maps based on droplet trajectory distribution, an assumption on the exhaled droplet size distribution must be made. Unfortunately in the literature there is not much agreement on this. In this work, a Pareto distribution of power 2 is assumed as suggested in [8]

$$\mathcal{N}\left(D_\mathrm{p}\right) = \frac{B}{D_\mathrm{p}^2} \tag{22}$$

Integrating equation (22) over a generic range of diameters $[D_\mathrm{min}, D_\mathrm{max}]$, the number of exhaled droplets in the range results

$$N_\mathrm{e} = \int_{D_\mathrm{min}}^{D_\mathrm{max}} \frac{B}{D_\mathrm{p}^2} = B\left(\frac{1}{D_\mathrm{min}} - \frac{1}{D_\mathrm{max}}\right) \tag{23}$$

whereas, by multiplying equation (22) for the droplet volume before integrating, the cumulative volume of the droplets in the same range is

$$V_\mathrm{e} = \frac{\pi B}{12}\left(D_\mathrm{max}^2 - D_\mathrm{min}^2\right) \tag{24}$$

The constant B can be computed as a function of the total droplet volume exhaled by performing the integration over the whole droplet size range of interest

$$B \approx \frac{12 V_\mathrm{e}}{\pi D_\mathrm{max}^2} \tag{25}$$

In the present work, as we deal with periodic respiratory events, the volume V_e should rather be intended as a volumetric flow rate. On the evaluation of this flow rate the literature is very sparse and the results given differ by orders of magnitude since the various studies are often focused on rather limited range of diameters and fail to give a comprehensive picture over the issue. By averaging the data provided in the review given in [16] a value of B=10^{-5} m/s has been chosen as most suitable for both the cases of breathing and speaking, the difference between the two respiratory events being in the droplet diameter range experimentally measured: from ≈0.1 µm to ≈5 µm for breathing, and from ≈0.1 µm to ≈1 mm for speaking. The droplet average volumetric flow rates that follow from equation (24) are 65.4 fl/s for breathing and 2.62 nl/s for speaking.

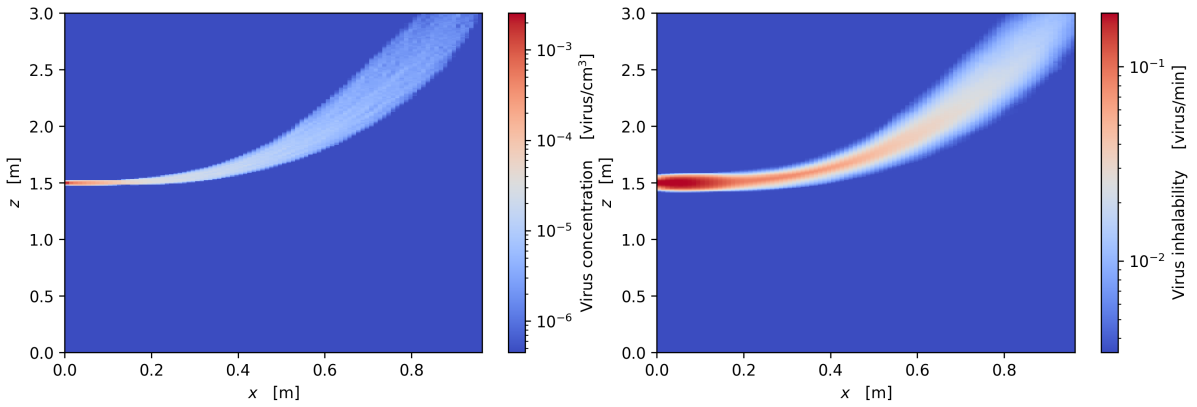

Figure 1. Virus concentration a) and inhalability b) in space for the case of mouth breathing.

The virus concentration in saliva samples can vary quite significantly during the course of an infectious disease. In [17] a value of c_s=120 copies/nl was estimated as a possible concentration in case of severe SARS-CoV-2 infection. This value is adopted in the post-processing of the simulation results that follow.

4. Results

The simulations described above have been post-processed to evaluate the virus concentration in the ambient and at the ground in front of a breathing or speaking infected individual.

Figure 1a) shows the virus concentration that is established in front of a mouth breathing infected individual. The figure is created by meshing the area in front of the individual's mouth with squared cells 1 cm in size. To each simulated droplet a diameter range and a viral load l

$$l = \frac{c_s V_e}{r} \tag{26}$$

are associated, where r is the number of simulation runs performed in each range. The trajectory of the droplet is then analysed and for each cell the droplet residence time t_r computed. The virus concentration in the cell is then evaluated as

$$c_c = \frac{t_r l}{V_c} \tag{27}$$

where V_c is the cell volume. Data in y direction is averaged over the jet amplitude to provide an easy to read 2D image. To the virus concentration thus computed, the concentration due to airborne droplet nuclei accumulating in the environment must be added. Droplet nuclei are assumed uniformly distributed, and, considering the virus half-life, their concentration at steady state depends on the emission rate and the room volume alone. Here a steady state concentration in a room of 100 m^3 with a severely infected breathing individual is assumed. The background concentration thus derived corresponds to the lower end value in the figure colour bar.

Figure 1b) shows the amount of virus inhaled by an individual staying with his nose or mouth for 1 minute in a certain relative position with respect to the emitter. The virus inhalability is computed by assuming 15 breathing cycles of 500 cm^3 per minute. The inhaled volume is assumed as an emisphere centred in the cell centre. Local inhaled air velocity in the neighbourhood is computed, and if the droplet trajectory intersects the emisphere with lower orthogonal velocity the droplet is assumed inhaled and its viral content is added to the count.

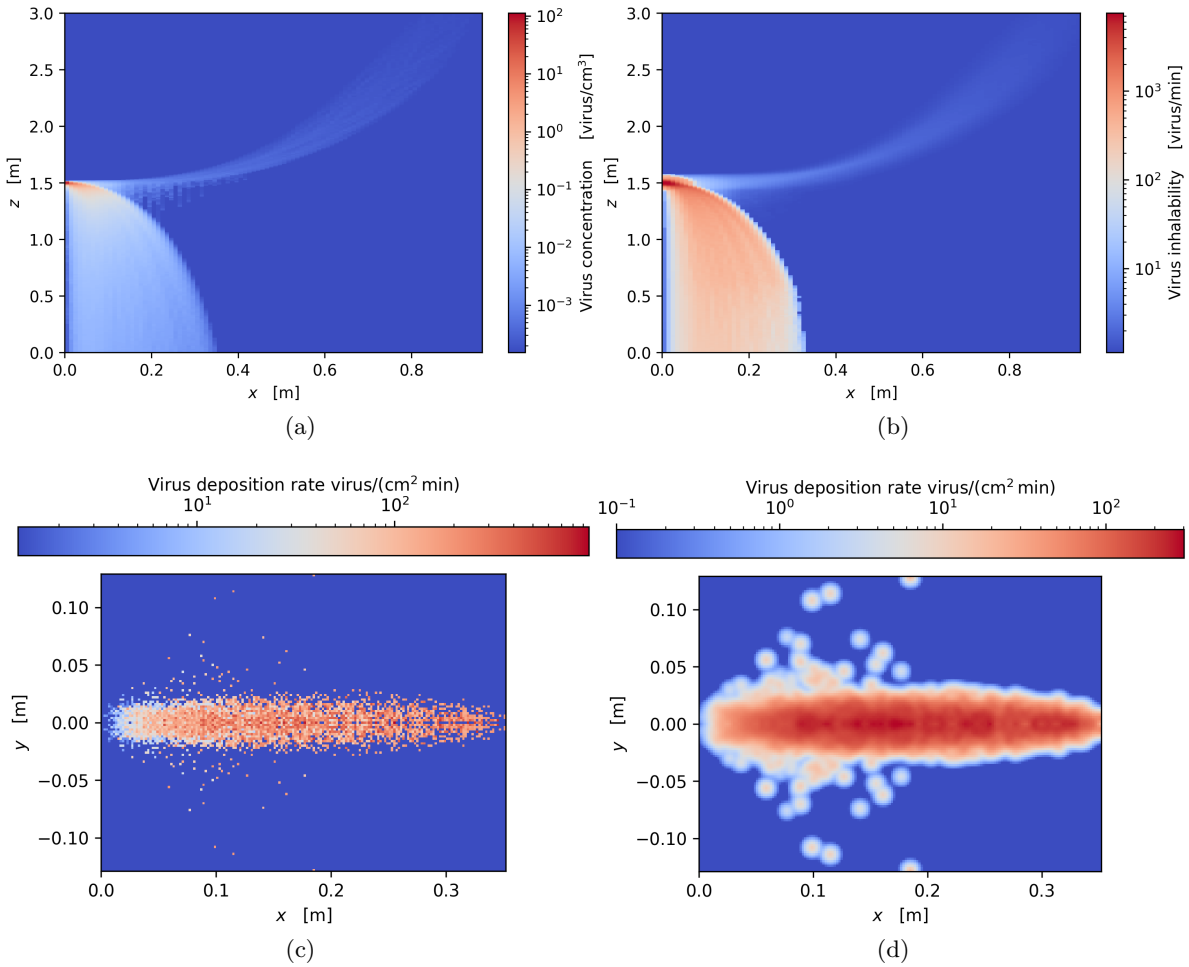

Figure 2. Virus concentration a) and inhalability b) in space, virus concentration c) and smoothed concentration d) at the ground for the case of speaking.

Figure 2 shows the same information for the case of speaking. The additional images represent the virus concentration accumulated per minute on the floor due to the dropets falling to the ground. In figure 2c) the ground in front of the infected speaker is meshed with squared cells 2 mm in size, and the viral load of each falling droplet added to the cell where the drop touches the ground. The image is then smoothed in figure 2d) to make it less dependent on the finite, although wide, number of simulations performed.

From figure 1 it can be seen that in case of breathing, due to the low amount of exhaled droplets in volume, virus concentration in the area in front of the infected individual and in the environment remains low. Nonetheless, if an individual is directly hit by someone's breath cloud, the risk of inhaling the virus grows exponentially becoming non-negligible in case of prolonged exposition. It must be reminded that, in case of SARS-CoV-2 infection, a dose of 50-100 virus has been estimated to be able to cause the disease with a probability of 63 % [18], a similar value to that is known for influenza. For the case of breathing, the 1 m rule seems to be confirmed even though barely sufficient to avoid any interaction with nearby individual's breath clouds.

Results for the case of speaking in figure 2a) and b) are qualitatively similar if not for the major contribution of the droplets falling to the ground to the overall virus concentration. More than 99% of the viruses exhaled, in fact, reach the ground, and less than 1% remain

airborne. Further, the much larger droplet volumetric flow rate translates into breath cloud and background virus concentrations more than two orders of magnitude higher compared to the previous case, so that the virus intake may become non-negligible even in case the proper social distancing is ensured, particularly in small environments.

The virus ground deposition rate in figure 2d) shows how the area interested by the droplet fall is limited to a distance of 30-40 cm from the speaker, yet the deposition rate can be as high as hundreds of viruses per square centimeter per minute. Considering that the virus half-life on surfaces is generally of the order of several hours, this shows the relevance also fomite transmission can have even days after the surface exposition to the virus.

5. Conclusions

An analytical model of exhaled droplet transport and evaporation has been used to draw preliminary infectious disease transmission risk maps based on virus concentration. The analytical tool implements a rather detailed empirical breath cloud model based on momentum conservation hypothesis, and features a discrete random walk model to account for the droplet turbulent dispersion, thus allowing statistical analyses to be made on the droplet trajectory, the falling distance, and the airborne fraction. The model has the advantage of a reduced computational cost compared to much more expensive discrete phase model CFD simulations.

A set of over 21 thousand simulations has been performed for the cases of mouth breathing and speaking. The maps obtained quantify the virus concentration in front of an infected individual, and thus the risks associated to direct and indirect airborne virus inhalation on behalf of a susceptible host. Further, they also quantify the virus concentration that may accumulate on the ground in front of a speaking individual and associated to indirect fomite transmission risk.

These preliminary results support the 1 m social distancing rule as being able to prevent direct inhalation route at least in case of breathing and speaking exhalations. On the other hand, indirect inhalation route may still be relevant, especially in case of an infected individual speaking in a small environment. Indirect fomite transmission has been shown to be also potentially relevant, even though the spatial range over which the exhaled droplets may fall to the ground is rather limited.

References

[1] Buonanno G, Stabile L and Morawska L 2020 *Environ Int* **141** 105794
[2] Pantelic J and Tham K 2012 *HVAC&R Res* **18** 562–574
[3] Busco G, Yang S, Seo J and Hassan Y 2020 *Phys Fluids* **32** 073309
[4] Li X, Shang Y, Yan Y, Yang L and Tu J 2018 *Build Environ* **128** 68–76
[5] Zeng G, Chen L, Yuan H, Yamamoto A and Maruyama S 2021 *Phys Fluids* **33** 123308
[6] Parienta D, Morawska L, Johnson G, Ristovski Z, Hargreaves M, Mengersen K, Corbett S, Chao C, Li Y and Katoshevski D 2011 *J Aerosol Sci* **42** 1–10
[7] Redrow J, Mao S, Celik I, Posada J and Feng Z G 2011 *Build Environ* **46** 2042–2051
[8] Balachandar S, Zaleski S, Soldati A, Ahmadi G and Bourouiba L 2020 *Int J Multiphas Flow* **132** 103439
[9] Wang H, Li Z, Zhang X, Zhu L, Liu Y and Wang S 2020 *Phys Fluids* **32** 125102
[10] Chen W, Zhang N, Wei J, Yen H L and Li W 2020 *Build Environ* **176** 106859
[11] Chao C, Wan M, Morawska L, Johnson G, Ristovski Z, Hargreaves M, Mengersen K, Corbett S, Li Y, Xie X and Katoshevski D 2009 *J Aerosol Sci* **40** 122–133
[12] Turner J S 1979 *Buoyancy effects in fluids* (Cambridge: Cambridge University Press)
[13] Wang B, Wu H and Wan X F 2020 *Phys Fluids* **32** 083307
[14] Wei J and Li Y 2015 *Build Environ* **93** 86–96
[15] Baturin V V 1972 *Fundamentals of industrial ventilation* (Oxford: Pergamon Press)
[16] Bourouiba L 2021 *Annu Rev Biomed Eng* **23** 547–577
[17] To K W, Tsang O Y, Yip C Y, Chan K H, Wu T C, Chan J C, Leung W S, Chik T H, Choi C C, Kandamby D, Lung D, Tam A, Poon R S, Fung A F, Hung I N, Cheng V C, Chan J W and Yuen K Y 2020 *Clin Infect Dis* **71** 841–843
[18] Kolinski J and Schneider T 2021 *Phys Rev E* **103** 033109